JACS
JOURNAL OF THE AMERICAN CHEMICAL SOCIETY
Article
Cite This: J. Am. Chem. Soc. 2018, 140, 11829−11835
pubs.acs.org/JACS

Building Strain with Large Macrocycles and Using It To Tune the Thermal Half-Lives of Hydrazone Photochromes

Quan Li, Hai Qian, Baihao Shao, Russell P. Hughes, and Ivan Aprahamian*

Department of Chemistry, Dartmouth College, Hanover, New Hampshire 03755, United States

Supporting Information

ABSTRACT: Strain has been used as a tool to modulate the reactivity (e.g., mechanochemistry) and thermal isomerization kinetics of photochromic compounds. Macrocyclization is used to build-up strain in such systems, and in general the reactivity and rates increase with the decrease in macrocycle size. To ascertain the effect of strain on recently reported bistable hydrazone photoswitches, we incorporated them into macrocycles having varying aliphatic linker lengths (**C3**−**C7**), and studied their switching behavior, and effect of macrocycle size on the thermal isomerization rate. Surprisingly, while the systems with **C3**−**C5** linkers behave as expected (i.e., the rate is faster with smaller linkers), the isomerization rate in the systems with larger aliphatic linkers (**C6**−**C8**) is enhanced up to 4 orders of magnitude. NMR spectroscopy, X-ray crystallography and DFT calculations were used to elucidate this unexpected behavior, which on the basis of our analyses results from the buildup of Pitzer (torsional), Prelog (transannular) and Baeyer (large angle) strain in the longer linkers.

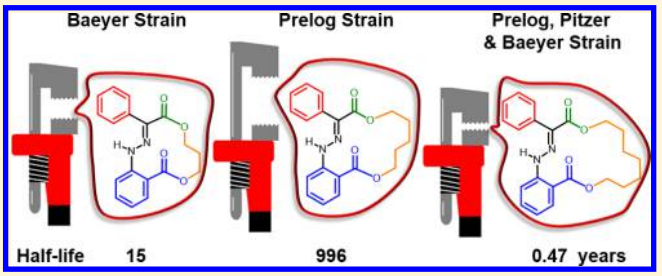

INTRODUCTION

Understanding how to build and control macrocyclic strain is an active research area, as it can be used in manipulating biological and chemical functions,[1] developing drugs[2] and synthesizing polymers,[3] among other applications. The numerous studies in this field led to the categorization of a number of factors that contribute to strained rings, which are (i) Baeyer or large angle strain, (ii) Pitzer or torsional strain, and (iii) Prelog or transannular strain.[4] The interplay of these factors plays an important role in determining the reactivity of macrocyclic systems, especially medium-ring compounds. A recent development in the field has been the incorporation of photochromic compounds[5] into macrocyclic systems[6] so that the photoinduced isomerization process can be used in tuning the strain, and hence reactivity, in the system.[7] These studies have led to a better understand of mechanochemistry,[8] allowed for the development of light-activated energy storage systems,[9] and the use of strain in manipulating the isomerization rates of the photochromic compounds.[10] It is this last aspect that interests us here.

The control over the isomerization rate of molecular switches, whether chemically or photochemically activated, has been extensively investigated as this property determines the function of the switch.[11] Recently, there has also been a push for the in situ modulation of rates using aggregation,[11g] electrochemistry,[12] and exchange reactions,[13] among others,[14] as such a control can eventually lead to the development of molecular clocks,[15] among other possibilities. In general though the tuning of the thermal half-life of molecular switches usually involves the synthetic manipulation of the chemical structure of the compound, to take advantage of electronic and/or steric effects in the de/acceleration of the thermal half-life. Another approach is the incorporation of the switches, especially photoswitches, into cyclic systems to take advantage of strain in accelerating isomerization rates.[10] For example, when stilbene is incorporated into a 17 membered ring it has a thermal relaxation half-life ($\tau_{1/2}$) of 17 days.[7a] However, when the macrocycle size is decreased to a 16 membered ring the $\tau_{1/2}$ drops sharply to only 100 ms. Similar effects can also be observed by changing the atom size in a macrocyclic system. For example, when exchanging the bridging sulfur atom in heterodiazocines to oxygen the half-life drops from 3.5 days at 27 °C to 89 s at 20 °C.[10f] These examples illustrate that the building up of even small amounts of strain through the exchange or removal of an atom can drastically accelerate the thermal half-lives of photoswitches.

These results have inspired us to try and use strain in controlling the isomerization rates of the bistable photochromic hydrazone switches[16] (thermal half-lives of up to 2700 years) that we recently reported on.[17] We took advantage of the facile synthesis of the hydrazone scaffold and incorporated it into macrocycles of varying sizes (**C3**−**C8**). The goal behind this approach was to use the strain generated by macrocyclization in accelerating, as is done usually,[10] the thermal isomerization rate. Herein, we report on the systematic study of the isomerization process of these macrocycles with an emphasis on the role that ring strain plays in controlling their thermal half-lives, which ranges from days to thousands of years. Surprisingly, it is the macrocycles with the larger ring

Received: July 18, 2018
Published: August 22, 2018

DOI: 10.1021/jacs.8b07612
J. Am. Chem. Soc. 2018, 140, 11829−11835

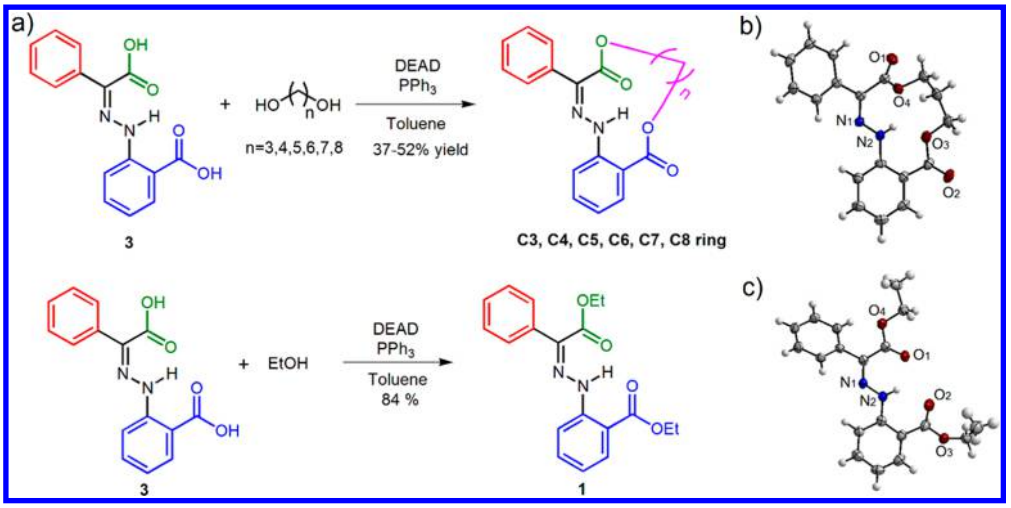

Figure 1. (a) Scheme of the synthesis of the hydrazone macrocycles **C3**−**C8** and the control compound **1**. The ORTEP drawing (50% probability) of the crystal structures of (b) **C3**-*Z* and (c) **1**-*Z* are also shown.

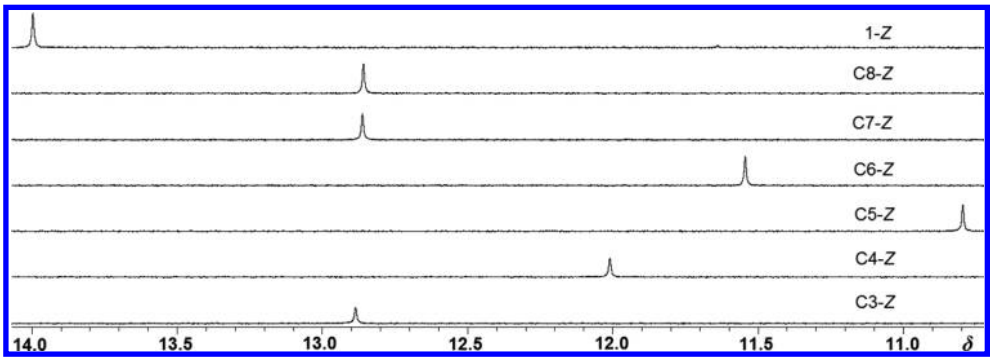

Figure 2. N−H proton resonances of the *Z* isomers of **1** and **C3**−**C8** in toluene-d_8.

sizes (**C6**−**C8**) that show orders of magnitude acceleration in isomerization rates.

RESULTS AND DISCUSSION

Synthesis and Characterization of the Photochromic Hydrazone Macrocycles. The photochromic macrocycles were synthesized in three easy steps (Figure 1a and Scheme S1), the key one being a Mitsunobu reaction between hydrazone **3** and the appropriate diol. The acyclic hydrazone **1**, bearing an ethyl ester group on both the rotor and stator parts of the switch (green and blue, respectively) was also synthesized as a control. The hydrazones were characterized using ^{1}H and ^{13}C NMR spectroscopies and X-ray crystallography. The ^{1}H NMR spectra (Figure 2) of the hydrazones show the characteristic low-field shifted N−H proton resonance, confirming the presence of an intramolecular H-bond in the molecules. While the N−H proton of **1** resonates at 14.00 ppm (indicating the presence of a strong intramolecular H-bond), the signals of **C3**-*Z*, **C4**-*Z* and **C5**-*Z* are relatively upfield shifted to 12.90, 12.00, and 10.80 ppm, respectively, indicating that the H-bond is steadily weakening in this series. The trend is reversed in **C6**-*Z*, **C7**-*Z*, and **C8**-*Z* as the N−H proton signal shifts to low-field (11.50, 12.86, and 12.85 ppm, respectively) indicating that the H-bond is getting stronger again, but nonetheless not as strong as in **1**.

An insight into this behavior comes from an analysis of the X-ray crystal structures of the switches (Figure 1b and Figure S118). The intramolecular H-bond is clearly evident in the solid state structures, and more importantly the nature of the bond is elucidated. In **C3**-*Z* and **C4**-*Z* the bifurcated bond is between the N−H proton and the two alkoxy oxygens (N_2−H···O_4, 2.59 Å, 132.2°; N_2−H···O_3, 2.56 Å, 134.4° for **C3**-*Z*; N_2−H···O_4, 2.65 Å, 127.3°; N_2−H···O_3, 2.66 Å, 129.2° for **C4**-*Z*). The longer bond lengths and smaller H-bond angle in **C4**-*Z* can explain the upfield shift observed in the ^{1}H NMR spectrum. In **C5**-*Z*, the stator (blue phenyl ring) N−H···O-alkoxy H-bond strength (N_2−H···O_3, 2.65 Å, 129.3°) is comparable to that in **C4**-*Z*; however, the N−H bond with the rotor part (green/red groups) is now with the ester carbonyl oxygen and is much weaker (N_2−H···O_4, 3.03 Å, 118.5°). This change in H-bonding partners explains why the N−H proton in **C5**-*Z* is the most upfield shifted. As for **C6**-*Z* and **C7**-*Z* (we could not get single crystals of **C8**-*Z*) the H-bond with the ester carbonyl in the rotor part is more optimal (N_2−H···O_1, 2.71, 133.3 and 2.62 Å, 129.1°, respectively) than in **C5**-*Z*, while the one with the stator (N_2−H···O_3, 2.68, 118.8 and 2.62 Å, 129.7°, respectively) is weaker and stronger, respectively, relative to **C4**-*Z*, contributing to the trend observed in the ^{1}H NMR spectrum.[18] On the basis of the ^{1}H NMR spectra and X-ray data analysis, it can be concluded that the nature and strength of the intramolecular H-bond in the hydrazones are largely dependent on the ring size, and the conformation of the ester groups, which is dictated by the conformation of the macrocycle.

Next, we employed UV−vis spectroscopy to study the photoisomerization of the hydrazones. An equilibrated aerated

DOI: 10.1021/jacs.8b07612
J. Am. Chem. Soc. 2018, 140, 11829−11835

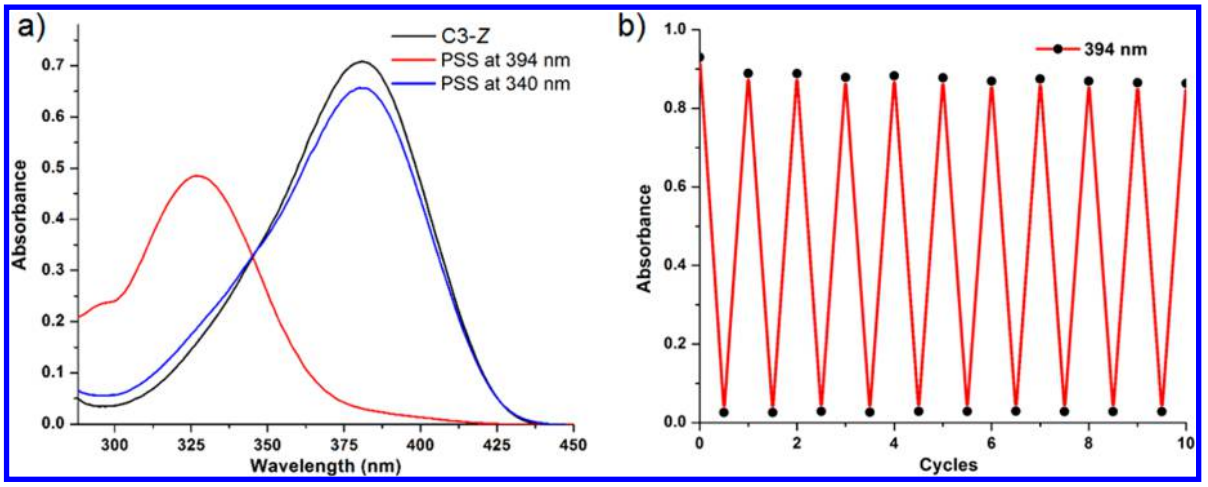

Figure 3. (a) Light induced *Z*/*E* isomerization of **C3** in toluene (3.0×10^{-5} M; aerated solution). (b) Switching cycles of **C3** upon alternating irradiation using 394 (ca. 2 min; 30 mW) and 340 (ca. 1 min; 20 mW) nm light sources. The absorbance change at 394 nm was monitored during the switching cycles.

Table 1. Kinetic Data and Activation Parameters for the Thermal Isomerization of the Hydrazone Switches in *p*-Xylene at 298 K[e]

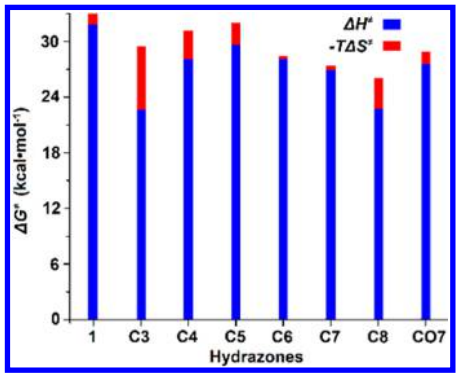

hydrazone	k[a] (s^{-1})	$\tau_{1/2}$[b] (year)	E_a (kcal·mol^{-1})	$\Delta H^{\ddagger}$[c] (kcal·mol^{-1})	$\Delta S^{\ddagger}$[c] (cal·mol^{-1}·K^{-1})	$\Delta G^{\ddagger}$[c] (kcal·mol^{-1})
1[d]	$(4.1 \pm 0.1) \times 10^{-12}$	5357 ± 101	32.7 ± 0.1	31.9 ± 0.1	−3.6 ± 0.1	32.9 ± 0.1
C3[d]	$(1.5 \pm 0.1) \times 10^{-9}$	15.0 ± 0.5	23.5 ± 0.1	22.7 ± 0.2	−22.6 ± 0.4	29.5 ± 0.3
C4[d]	$(9.9 \pm 0.5) \times 10^{-11}$	223 ± 10	28.8 ± 0.1	28.1 ± 0.1	−10.2 ± 0.2	31.1 ± 0.1
C5[d]	$(2.2 \pm 0.1) \times 10^{-11}$	996 ± 67	30.4 ± 0.2	29.7 ± 0.2	−7.6 ± 0.6	31.9 ± 0.4
C6[d]	$(9.1 \pm 0.7) \times 10^{-9}$	2.42 ± 0.19	28.8 ± 0.2	28.1 ± 0.2	−1.1 ± 0.6	28.4 ± 0.4
C7[d]	$(4.8 \pm 0.4) \times 10^{-8}$	0.46 ± 0.04	27.6 ± 0.3	26.9 ± 0.3	−1.6 ± 0.8	27.4 ± 0.5
C8[d]	$(4.7 \pm 0.5) \times 10^{-7}$	0.047 ± 0.005	23.5 ± 0.4	22.8 ± 0.4	−10.9 ± 1.0	26.1 ± 0.7
CO7[d]	$(4.3 \pm 0.2) \times 10^{-9}$	5.1 ± 0.28	28.3 ± 0.1	27.6 ± 0.1	−4.2 ± 0.3	28.8 ± 0.2

[a]The first-order rate constants at 298 K calculated using the Arrhenius equation. [b]Half-life. [c]The thermodynamic parameters of activation calculated using the Eyring equation. [d]Thermal relaxation occurs from $E \rightarrow Z$. [e]The inset is a graphical depiction of the contributions of $\Delta H^{\ddagger}$ and $\Delta S^{\ddagger}$ to the energy barrier.

toluene solution of **C3**-*Z*, for example, shows a maximum absorbance (λ_{max}) at 381 nm (molar attenuation coefficient (ε) of 25 300 $M^{-1}\cdot cm^{-1}$), which shifts hypsochromically to 327 nm upon irradiation with 394 nm light and isomerization to the *E* form. Switch **C3**-*E* (λ_{max} = 327 nm, ε = 18 900 $M^{-1}\cdot cm^{-1}$) could be converted back to its *Z* form upon irradiation with 340 nm light (Figure 3a). The photoisomerization efficiency of **C3** was studied using ^{1}H NMR spectroscopy. Irradiation with 394 nm light yields a photostationary state (PSS) consisting of >99% **C3**-*E*, which then yields a PSS_{340} consisting of 90% **C3**-*Z* upon 340 nm light irradiation. The photoisomerization quantum yields of the $Z \rightarrow E$ and $E \rightarrow Z$ processes were determined to be 3.4 ± 0.3 and 9.2 ± 0.5%, respectively (Figure S48−S61, Table S3).[19] Similarly, macrocycles **C4**-*Z*, **C5**-*Z*, **C6**-*Z*, **C7**-*Z* and **C8**-*Z* could be switched to their *E* isomers nearly quantitatively with 394 nm light irradiation (Figure S35−S40,Table S2). Noticeably, the λ_{max} for **C3**-*E*, **C4**-*E*, **C5**-*E*, **C6**-*E*, **C7**-*E* and **C8**-*E* at PSS does not differ significantly. This suggests that all of the *E* isomers in this series possess a similar π-conjugation. The resilience of these macrocyclic hydrazones was also studied, and no significant signs of fatigue were observed up to 10 isomerization cycles (Figure 3B and Figure S42−S47). These results confirm the robustness of all these novel photochromic cyclic structures.

Thermal Half-Lives. One of the most important features of this newly developed family of photochromic switches[17] is their extremely long thermal half-lives. As mentioned earlier, the aim of incorporating the switch into a macrocyclic

DOI: 10.1021/jacs.8b07612
J. Am. Chem. Soc. 2018, 140, 11829−11835

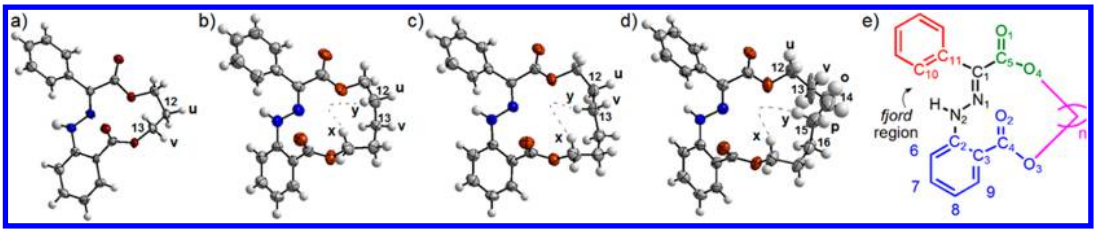

Figure 4. X-ray structures of (a) **C3**-*E*, (b) **C5**-*E*, (c) **C6**-*E*, (d) **C7**-*E* (all the structures are drawn in ORTEP at 50% probability). (e) Scheme depicting the key atoms that will be used in discussing the X-ray and NMR data of the *E* hydrazones. Only one of the structures in the unit cell (crystal structure 1 (CS1)) of **C3**-*E*, **C6**-*E*, and **C7**-*E* is shown. There is disorder in the aliphatic section of **C5**-*E* and so only one of the structures is shown. The other structures (CS2) can be found in Figure S119.

structure was to take advantage of ring-size dependent strain in tuning/accelerating the thermal isomerization rate. To test this premises, we measured the isomerization rates of all the *E* macrocyclic hydrazones in *p*-xylene at various temperatures.[20] The extrapolation of the obtained Arrhenius plot yielded the thermal half-lives of the switches at room temperature. The activation parameters for the thermal isomerization process were obtained using Eyring plots (Table 1, Figure S62−S117 in Supporting Information).

We will start with the acyclic hydrazone **1**, which has the largest energy barrier measured thus far for these systems, and a subsequent thermal half-life of 5357 ± 101 years (Table 1), which is almost double the value reported for the original system (2700 years).[15] Although there is a minor entropic contribution to the energy barrier ($\Delta S^{\ddagger}$ = −3.6 ± 0.1 cal·mol^{-1}·K^{-1}), the lion share of the effect is enthalpic ($\Delta H^{\ddagger}$ = 31.9 ± 0.1 kcal·mol^{-1}), which is attributed to the presence of an additional intramolecular H-bond with the stator phenyl group (i.e., blue ring). In the original system this bond was with a quinolinyl subunit and formed a five membered ring, here the intramolecular H-bond forms a six-membered ring and hence is stronger leading to the larger barrier. We hypothesize that the intramolecular H-bond hampers access to the linear transition state required in the inversion mechanism (vide infra) leading to the larger activation barrier. This assumption is validated by our previous result that shows a much faster isomerization rate (10-fold decrease of half-life) in the absence of the additional intramolecular H-bond.[15]

The half-lives for **C3**-*E*, **C4**-*E* and **C5**-*E* are somewhat shorter than in **1**, but are still in the 10−1000 years range (Table 1). The data show that the acceleration in thermal isomerization rate (1−3 orders of magnitude going from **C5**-**C3**) are governed by both enthalpy and entropy. The large negative $\Delta S^{\ddagger}$ value (−22.6 ± 0.4 cal·mol^{-1}·K^{-1}) in **C3** may suggest a more ordered structure and less conformational freedom in the transition state because of the rigidity of the smaller ring. As the size of the ring increases in **C4**-*E* and **C5**-*E*, the $\Delta S^{\ddagger}$ value also increases to −10.2 ± 0.2 and −7.6 ± 0.6 cal·mol^{-1}·K^{-1}, respectively. This may indicate an increased disorder in the transition state because of the flexibility of the larger rings. Simultaneously, the $\Delta H^{\ddagger}$ value increases going from **C3**-*E* (22.7 ± 0.2 kcal·mol^{-1}) to **C5**-*E* (29.7 ± 0.2 kcal·mol^{-1}), suggesting that there is less strain in the larger system and a more stabilized ground state. These two effects together lead to a decrease in the half-life of these macrocycles as a function of ring size relative to **1**, which has no strain and less geometrical constraints leading to higher $\Delta H^{\ddagger}$ and $\Delta S^{\ddagger}$ values.

To our surprise, switches **C6**-*E*, **C7**-*E* and **C8**-*E* have strikingly short half-lives of 2.42 ± 0.19, 0.46 ± 0.04 and 0.047 ± 0.005 years, respectively. That is, the isomerization rate is *increasing* with ring size, which is counterintuitive. Analysis of the thermodynamic data (Table 1) shows a decrease in both the $\Delta S^{\ddagger}$ and $\Delta H^{\ddagger}$ values going from **C6**-*E* to **C8**-*E* implying that enthalpy and entropy are again playing a role in the overall rate control. The decrease in $\Delta H^{\ddagger}$ value indicates that there is destabilization in the switches as we go to larger rings, whereas the relative decrease in $\Delta S^{\ddagger}$ values in **C8**-*E* vs **C6**-*E* and **C7**-*E* means that there is more disorder in the transition state of the latter two than the former. These two trends explain in general the acceleration of isomerization rate in these three systems vs **1**-*E* and **C3**-*E*−**C5**-*E*. When comparing the macrocycles themselves the effect of entropy becomes evident. For example, **C3**-*E* and **C8**-*E* have the same $\Delta H^{\ddagger}$ value; however the $\Delta S^{\ddagger}$ value is almost half leading to a two-order magnitude increase in isomerization rate. Again, what is strange here is the fact that the systems with smaller rings, and hence more apparent strain, and larger ones, which should be less strained, have the same ground state stabilization energy.

X-ray Analysis. To interpret the above-mentioned ring size/thermal half-life relationship, we analyzed the crystal structures of **C3**-*E*, **C5**-*E*, **C6**-*E* and **C7**-*E* (we could not grow crystals of **C4**-*E* and **C8**-*E* that were suitable for X-ray crystallography analysis; Figure 4).

For **C3**-*E* and **C5**-*E* we first investigated the effect of macrocyclization on the C═N—N hydrazone unit, which is responsible for the isomerization process. The $\angle C_1-N_1-N_2$ and $\angle N_1-N_2-C_2$ angles in **C3**-*E* were measured to be 124.8° and 115.5°, respectively, in one of the structures in the unit cell (crystal structure 1 (CS1)), and 124.1° and 116.0°, respectively, in the second structure (crystal structure 2 (CS2)), while in **C5**-*E* the values are 118.4° and 118.3°, respectively. On the basis of this data it could be inferred that the $C_1-N_1-N_2$ bond in **C3**-*E* is bent/pulled toward the center of the ring as a result of the strain generated by the small ring. This bending of the bond brings it closer to the linear transition state required in the inversion mechanism (vide infra) and might explain why the overall energy barrier in **C3**-*E* is smaller than in **C4**-*E* and **C5**-*E*. As for the aliphatic ring both **C3**-*E* (dihedral angle of −34.9° (CS1) and 33.2° (CS2) for $H_u-C_{12}-C_{13}-H_v$) and **C5**-*E* (dihedral angle of −34.7° for $H_u-C_{12}-C_{13}-H_v$) have some torsional strain, while **C5**-*E* also has Prelog (transannular) strain (distance of 2.10 Å and 2.35 Å between H_x and H_y in CS1 and CS2, respectively; Figure 4b and Figure S119b in Supporting Information). This analysis indicates that the acceleration in rate in **C3**-*E* is mainly coming from the angle strain mentioned above.

Next, we analyzed the crystal structures of **C6**-*E* and **C7**-*E*. Both compounds have similar $\angle C_1-N_1-N_2$ and $\angle N_1-N_2-C_2$ angles (116.9°, 118.7° in CS1 and 117.8°, 117.7° in CS2 for **C6**-*E*; 118.0°, 118.3° in CS1 and 117.1°, 118.3° in CS2 for **C7**-

DOI: 10.1021/jacs.8b07612
J. Am. Chem. Soc. 2018, 140, 11829−11835

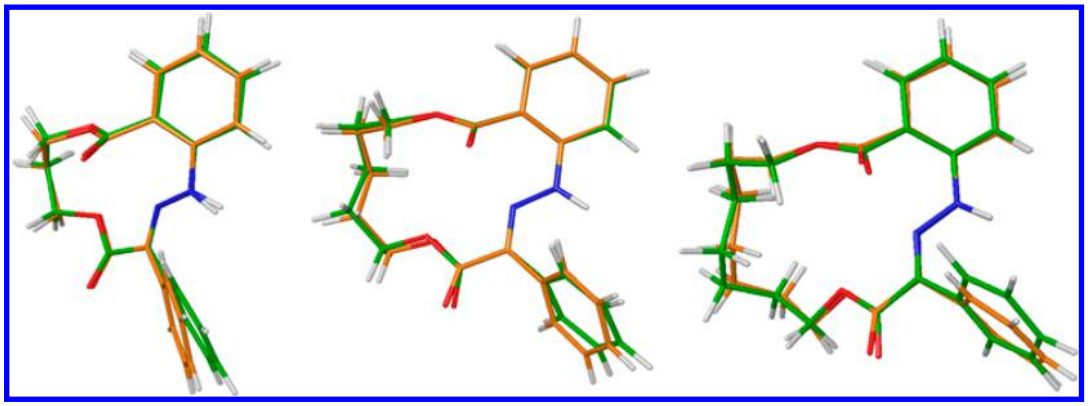

Figure 5. Superposition of the crystallographic (orange) and DFT calculated (green) structures of (from left to right) **C3**-*E*, **C5**-*E* and **C7**-*E*.

E) to that measured in **C5**-*E* indicating that the difference in rate is not emanating from angle strain in the hydrazone moiety. Hence, our focus turned to the aliphatic chain. Compounds **C6**-*E* has one partially eclipsed bonds (dihedral angle of 33.7° for $H_u-C_{12}-C_{13}-H_v$) in one of its structures (Figure 4c), while **C7**-*E* has two such eclipsed bonds (dihedral angle of 17.1° and −32.9° for $H_u-C_{12}-C_{13}-H_v$ and $H_o-C_{14}-C_{15}-H_p$) in one of its structures indicating the presence or Pitzer strain in the system. As for Prelog strain **C6**-*E* has one short contact between hydrogens H_x and H_y (2.14 Å) (Figure 4c) while **C7**-*E* has two such contacts (a distance of 2.26 Å was measured for the H_x and H_y hydrogens in CS1; 2.16 Å between H_x and H_y and 2.37 Å between H_y and H_z in CS2) (Figure 4d and Figure S119d in the Supporting Information). Lastly both compounds have Baeyer strain with angles as large as 122.0° ($\angle C_{12}-C_{13}-C_{14}$ in CS2, Figure S119c in Supporting Information) and 120.1° ($\angle C_{14}-C_{15}-C_{16}$ in CS1, Figure 4d) for **C6**-*E* and **C7**-*E*, respectively. This analysis shows a buildup in transannular, torsional and large angle strain when going from **C5**-*E* to **C7**-*E*, which can explain the unusual acceleration in isomerization rate upon increase in macrocycle size. Moreover, it seems that the large angle strain in addition to the accumulation of torsional strain is responsible for the disparity in thermal half-lives between the smaller and larger macrocycles.

On the basis of this analysis, it could be hypothesized that suppression of the factors leading to strain in the macrocyclic ring will increase the thermal half-life of the switches. To test this hypothesis, we synthesized the control compound **CO7** in which the central methylene group of a C7 aliphatic chain is replaced with an oxygen atom (see Scheme S2). We presumed that this structural alteration will relieve the torsional, transannular and large angle strain in the system, and yield a longer thermal half-life than in **C7**. Indeed, the kinetic data show that **CO7**-*E* has a thermal half-life of ca. 5 years vs 0.5 years in **C7**-*E* (Table 1). Analysis of the crystal structure of **CO7**-*E* (Figure S119e in Supporting Information) shows that the main culprit in the 10-fold increase in thermal half-life is the fact that there is no large angle strain or Pitzer strain in the system. Only Prelog strain (distance of 2.26 Å between hydrogens H_x and H_y) can be found in the system. This result unambiguously demonstrates that buildup of torsional, transannular and angle strain in the larger macrocycles results in isomerization rate acceleration.

One point of consideration when dealing with crystal structure analysis is whether it represents the structure in solution. We used ^{1}H and ^{13}C NMR spectroscopies to gain insight into this point. The N−H proton signal of **C3**-*E* resonates at 7.92 ppm and shifts upfield throughout the series until it reaches 7.71 ppm in **C7**-*E*. This trend in upfield shift correlates well with the increase observed in the $C_{10}-C_{11}-C_1-N_1$ dihedral angle (Figure 4e), which changes from 41.4° to 73.6° in CS1 (−39.9° to 59.8° in CS2) going from **C3**-*E* to **C7**-*E*, respectively. This angle is a measure of the coplanarity of the phenyl group in the rotor part with the rest of the molecule. The larger the angle the more shielding effect the phenyl group will exert on the *fjord* region (Figure 4e). This is indeed what we are seeing in solution as the N−H proton signal is shifting upfield. Another probe that can be used in detecting conformational changes in the macrocyclic structures is the $C_2-C_3-C_4-O_2$ dihedral angle. This angle decreases going from **C3**-*E* to **C7**-*E* (59.7° to 50.9° in CS1; −62.2° to 52.4° in CS2) indicating that the carbonyl group is becoming more coplanar with the stator phenyl group, which should lead to more deshielding of the phenyl group. This effect is observed in the ^{13}C NMR chemical shifts of the lower benzene moiety (Figure 4e, table S1). For example, the chemical shifts of carbon C6 shifts downfield going from **C3**-*E* to **C7**-*E* (115.78 and 119.71 ppm, respectively) as the dihedral angle decreases. The same trend is also observed for carbons C7 and C9. The fairly good agreement between the crystal and solution NMR data in the above analysis lends credence to our ability to use the solid-state crystal structure analyses in interpreting the solution thermal half-lives.

DFT Calculations. In an attempt to shed some further light on the isomerization mechanism and unusual effect of ring size on the thermal $E \rightarrow Z$ isomerization rate, DFT calculations were carried out on the macrocycles using the M06 functional and the 6-311G**++ basis set. A continuum Poisson−Boltzmann solvent model (benzene) was used during the calculations. Full details are provided in the Supporting Information). The DFT calculations do a good job of matching metrics and conformational properties with those determined crystallographically; overlays of the calculated **C3**-*E*, **C5**-*E* and **C7**-*E* structures with their crystallographic versions are shown in Figure 5.

Two pathways were considered for the $E \rightarrow Z$ isomerization process in the switches.[21] A direct isomerization by rotation about the C═N double bond was quickly discounted, since the activation free energies for this process in all systems were 35−45 kcal/mol above the corresponding measured energy of the systems. The other option considered is an inversion at the N−N bond, via a linear CNN transition state, to give the *E* isomer invertomer shown in Scheme 1, subsequent N−N

DOI: 10.1021/jacs.8b07612
J. Am. Chem. Soc. 2018, 140, 11829−11835

Scheme 1. N−N Inversion and Rotation Pathways for the *E* → *Z* Isomerization Process[a]

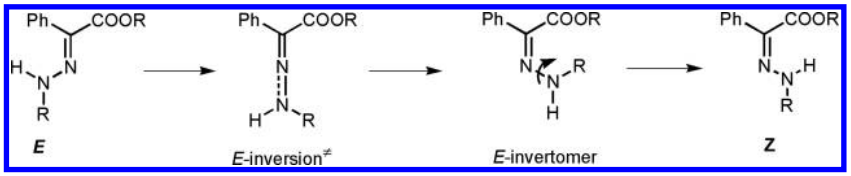

[a]Acyclic structures are drawn for clarity, but in the real systems the R groups are linked to form the cyclic structures.

rotation affords the Z-isomer. All N−N rotational barriers were found to be small (ca. 7−10 kcal/mol) compared to the inversion barrier; the latter would clearly be rate limiting. Regardless of any mechanistic pathway prediction, the DFT results do not compare well with the experimentally obtained $\Delta G^{\ddagger}$ values (Table 1 and Table S20 in Supporting Information) as the calculated values are significantly lower than those observed experimentally, except for in **C7**-*E*. These results highlight the difficulty in calculating the properties of macrocyclic systems having large degrees of conformational freedom, especially when coupled to isomerization mechanisms that do not necessarily need to be pure rotation or inversion. At this stage our conclusion is that the isomerization mechanism is not rotation, and might be mainly inversion with a rotational component. Further studies are necessary to pinpoint the exact isomerization mechanism in these systems.

We also performed isodesmic reaction calculations[22] (Scheme S3) to estimate the strain energy that is stored in the macrocycles. The difference (Q) in heats of formation (ΔH_f°) between the reactants and products represents the energetic penalty (strain energy) that needs to be paid to form the cyclic structure (Table S21). The calculations showed that **C3**-*E* was destabilized ($Q < 0$) by 0.2 kcal·mol^{-1} relative to its acyclic form. However, **C4**-*E* and **C5**-*E* were stabilized ($Q > 0$) by 2.2, and 4.0 kcal·mol^{-1}, respectively, relative to their acyclic form. This calculated stability trend among **C3**-*E*, **C4**-*E* and **C5**-*E* is consistent with their thermal half-life changes. As for **C6**-*E*, its Q value drops to 0.4 kcal·mol^{-1} which is much smaller than in **C5**-*E* reflecting a significant decrease in thermal stability. The Q value for **C7**-*E* and **C8**-*E* are similar to that found in **C4**-*E* suggesting a similar strain which is contradictory to the experimental results. This unusual result may be attributed to the conformational freedom in the larger rings (**C6**-*E*, **C7**-*E* and **C8**-*E*), which as discussed earlier are difficult to properly predict computationally as illustrated in the comparison between X-ray and computational structures in Figure 5. However, our calculations still predict that the thermal half-life changes in **C3**-*E*, **C4**-*E*, **C5**-*E* and **C6**-*E*, **C7**-*E*, **C8**-*E* follow different scenarios. Again further studies and more in-depth calculations will be necessary to elaborate on these discrepancies particularly for **C6**-*E*, **C7**-*E* and **C8**-*E*.

CONCLUSIONS

Here we present a systematic study on the effect of ring size on the thermal isomerization rate of a bistable hydrazone-based photochromic compound. The thermal half-life of the hydrazone changes as a function of ring size. When going from a **C3** linker to a **C5** linker the rate follows the expected trend based on angle strain, that is it becomes slower as there is less strain in the system. However, a more substantial rate acceleration occurs with the larger (**C6**−**C8**) linkers. We attribute this to a combination of Prelog, Pitzer and Baeyer strain that increases the energy of the system relative to the acyclic system, and without the counterbalance of entropic penalty that is found in the smaller linkers, leads to the observed phenomenon. These findings are informative as they open the way for using larger rings in mechanochemistry.[8] Currently there is a focus on utilizing the strain in smaller rings for such applications, and these results show that substantial strain can also be induced with larger ones.

ASSOCIATED CONTENT

Supporting Information

The Supporting Information is available free of charge on the ACS Publications website at DOI: 10.1021/jacs.8b07612.

General methods, experimental procedures, NMR spectra of compounds, photoisomerization studies, kinetic studies, crystal structures, and DFT calculations (PDF)

Crystallographic data for **1**-*Z* (CIF)

Crystallographic data for **C3**-*Z* (CIF)

Crystallographic data for **C4**-*Z* (CIF)

Crystallographic data for **C5**-*Z* (CIF)

Crystallographic data for **C6**-*Z* (CIF)

Crystallographic data for **C7**-*Z* (CIF)

Crystallographic data for **C3**-*E* (CIF)

Crystallographic data for **C5**-*E* (CIF)

Crystallographic data for **C6**-*E* (CIF)

Crystallographic data for **C7**-*E* (CIF)

Crystallographic data for **CO7**-*E* (CIF)

AUTHOR INFORMATION

Corresponding Author

*ivan.aprahamian@dartmouth.edu

ORCID

Ivan Aprahamian: 0000-0003-2399-8208

Notes

The authors declare no competing financial interest.

ACKNOWLEDGMENTS

I.A. is grateful to the NSF (CHE-1807428) for generous support. We gratefully acknowledge Prof. Richard Staples (Michigan State University) for X-ray data processing.

REFERENCES

(1) (a) Casadei, M. A.; Galli, C.; Mandolini, L. *J. Am. Chem. Soc.* **1984**, *106*, 1051−1056. (b) Galli, C.; Mandolini, L. *Eur. J. Org. Chem.* **2000**, *2000*, 3117−2312. (c) Agard, N. J.; Prescher, J. A.; Bertozzi, C. R. *J. Am. Chem. Soc.* **2004**, *126*, 15046−15047. (d) Bogdan, A. R.; Jerome, S. V.; Houk, K. N.; James, K. *J. Am. Chem. Soc.* **2012**, *134*, 2127−2138. (e) Babii, O.; Afonin, S.; Berditsch, M.; Reier, S.; Mykhailiuk, P. K.; Kubyshkin, V. S.; Steinbrecher, T.; Ulrich, A. S.; Komarov, I. V. *Angew. Chem., Int. Ed.* **2014**, *53*, 3392−3395. (f) Yudin, A. K. *Chem. Sci.* **2015**, *6*, 30−49. (g) Walczak, M. A. A.; Krainz, T.; Wipf, P. *Acc. Chem. Res.* **2015**, *48*, 1149−1158. (h) Martí-

DOI: 10.1021/jacs.8b07612
J. Am. Chem. Soc. 2018, 140, 11829−11835

Centelles, V.; Pandey, M. D.; Burguete, M. I.; Luis, S. V. *Chem. Rev.* **2015**, *115*, 8736−8834.
(2) (a) Oyelere, A. K. *Curr. Top. Med. Chem.* **2010**, *10*, 1359−1360. (b) Levin, J. *Macrocycles in Drug Discovery*; Royal Society of Chemistry: Cambridge, UK, 2015.
(3) (a) Hall, H. K. *J. Am. Chem. Soc.* **1958**, *80*, 6412−6420. (b) Wright, M. E.; Allred, G. D.; Wardle, R. B.; Cannizzo, L. F. *J. Org. Chem.* **1993**, *58*, 4122−4126. (c) Robb, M. J.; Kim, T. A.; Halmes, A. J.; White, S. R.; Sottos, N. R.; Moore, J. S. *J. Am. Chem. Soc.* **2016**, *138*, 12328−12331. (d) Larsen, M. B.; Boydston, A. J. *Macromol. Chem. Phys.* **2016**, *217*, 354−364. (e) Chen, Z.; Mercer, J. A. M.; Zhu, X.; Romaniuk, J. A. H.; Pfattner, R.; Cegelski, L.; Martinez, T. J.; Burns, N. Z.; Xia, Y. *Science* **2017**, *357*, 475−479.
(4) (a) Wiberg, K. B. *Angew. Chem., Int. Ed. Engl.* **1986**, *25*, 312−322. (b) Anslyn, E. V.; Dougherty, D. A. *Modern Physical Organic Chemistry*; University Science: Sausalito, CA, 2006; pp 100−109.
(5) (a) Beharry, A. A.; Woolley, G. A. *Chem. Soc. Rev.* **2011**, *40*, 4422−4437. (b) Bandara, H. M. D.; Burdette, S. C. *Chem. Soc. Rev.* **2012**, *41*, 1809−1825. (c) Irie, M.; Fukaminato, T.; Matsuda, K.; Kobatake, S. *Chem. Rev.* **2014**, *114*, 12174−12277. (d) Klajn, R. *Chem. Soc. Rev.* **2014**, *43*, 148−184. (e) Harris, J. D.; Moran, M. J.; Aprahamian, I. *Proc. Natl. Acad. Sci. U. S. A.* **2018**, 201714499.
(6) (a) Shinkai, S.; Nakaji, T.; Nishida, Y.; Ogawa, T.; Manabe, O. *J. Am. Chem. Soc.* **1980**, *102*, 5860−5865. (b) Boeckmann, K.; Voegtle, F. *Chem. Ber.* **1981**, *114*, 1065−1073. (c) Norikane, Y.; Kitamoto, K.; Tamaoki, N. *Org. Lett.* **2002**, *4*, 3907−3910. (d) Mathews, M.; Tamaoki, N. *J. Am. Chem. Soc.* **2008**, *130*, 11409−11416.
(7) (a) Huang, Z.; Yang, Q. Z.; Khvostichenko, D.; Kucharski, T. J.; Chen, J.; Boulatov, R. *J. Am. Chem. Soc.* **2009**, *131*, 1407−1409. (b) Kucharski, T. J.; Yang, Q. Z.; Tian, Y. C.; Boulatov, R. *J. Phys. Chem. Lett.* **2010**, *1*, 2820−2825. (c) Akbulatov, S.; Tian, Y. C.; Huang, Z.; Kucharski, T. J.; Yang, Q. Z.; Boulatov, R. *Science* **2017**, *357*, 299−303. (d) Wagner-Wysiecka, E.; Łukasik, N.; Biernat, J. F.; Luboch, E. *J. Inclusion Phenom. Macrocyclic Chem.* **2018**, *90*, 189−257.
(8) (a) Balaz, P.; Achimovicova, M.; Balaz, M.; Billik, P.; Cherkezova-Zheleva, Z.; Criado, J. M.; Delogu, F.; Dutkova, E.; Gaffet, E.; Gotor, F. J.; Kumar, R.; Mitov, I.; Rojac, T.; Senna, M.; Streletskii, A.; Wieczorek-Ciurowa, K. *Chem. Soc. Rev.* **2013**, *42*, 7571−7637. (b) Li, J.; Nagamani, C.; Moore, J. S. *Acc. Chem. Res.* **2015**, *48*, 2181−2190. (c) Akbulatov, S.; Boulatov, R. *ChemPhysChem* **2017**, *18*, 1422−1450.
(9) (a) Kanai, Y.; Srinivasan, V.; Meier, S. K.; Vollhardt, K. P. C.; Grossman, J. C. *Angew. Chem., Int. Ed.* **2010**, *49*, 8926−8929. (b) Kucharski, T. J.; Tian, Y.; Akbulatov, S.; Boulatov, R. *Energy Environ. Sci.* **2011**, *4*, 4449−4472. (c) Durgun, E.; Grossman, J. C. *J. Phys. Chem. Lett.* **2013**, *4*, 854−860. (d) Vlasceanu, A.; Broman, S. L.; Hansen, A. S.; Skov, A. B.; Cacciarini, M.; Kadziola, A.; Kjaergaard, H. G.; Mikkelsen, K. V.; Nielsen, M. B. *Chem. - Eur. J.* **2016**, *22*, 10796−10800. (e) Vlasceanu, A.; Frandsen, B. N.; Skov, A. B.; Hansen, A. S.; Rasmussen, M. G.; Kjaergaard, H. G.; Mikkelsen, K. V.; Nielsen, M. B. *J. Org. Chem.* **2017**, *82*, 10398−10407. (f) Heindl, A. H.; Schweighauser, L.; Logemann, C.; Wegner, H. A. *Synthesis* **2017**, *49*, 2632−2639.
(10) (a) Röttger, D.; Rau, H. *J. Photochem. Photobiol., A* **1996**, *101*, 205−214. (b) Nagamani, S. A.; Norikane, Y.; Tamaoki, N. *J. Org. Chem.* **2005**, *70*, 9304−9313. (c) Norikane, Y.; Tamaoki, N. *Eur. J. Org. Chem.* **2006**, *5*, 1296−1302. (d) Bassotti, E.; Carbone, P.; Credi, A.; Stefano, M. D.; Masiero, S.; Negri, F.; Orlandi, G.; Spada, G. P. *J. Phys. Chem. A* **2006**, *110*, 12385−12394. (e) Schweighauser, L.; Häussinger, D.; Neuburger, M.; Wegner, H. A. *Org. Biomol. Chem.* **2014**, *12*, 3371−3379. (f) Hammerich, M.; Schütt, C.; Stähler, C.; Lentes, P.; Röhricht, F.; Höppner, R.; Herges, R. *J. Am. Chem. Soc.* **2016**, *138*, 13111−13114.
(11) (a) Irie, M. *Chem. Rev.* **2000**, *100*, 1685−1716. (b) Pollard, M. M.; Klok, M.; Pijper, D.; Feringa, B. L. *Adv. Funct. Mater.* **2007**, *17*, 718−729. (c) Su, X.; Aprahamian, I. *Org. Lett.* **2011**, *13*, 30−33. (d) Bléger, D.; Schwarz, J.; Brouwer, A. M.; Hecht, S. *J. Am. Chem. Soc.* **2012**, *134*, 20597−20600. (e) Su, X.; Aprahamian, I. *Org. Lett.* **2013**, *15*, 5952−5955. (f) Weston, C. E.; Richardson, R. D.; Haycock, P. R.; White, A. J. P.; Fuchter, M. J. *J. Am. Chem. Soc.* **2014**, *136*, 11878−11881. (g) Qian, H.; Wang, Y. Y.; Guo, D. S.; Aprahamian, I. *J. Am. Chem. Soc.* **2017**, *139*, 1037−1040.
(12) Goulet-Hanssens, A.; Utecht, M.; Mutruc, D.; Titov, E.; Schwarz, J.; Grubert, L.; Bleger, D.; Saalfrank, P.; Hecht, S. *J. Am. Chem. Soc.* **2017**, *139*, 335−341.
(13) Cvrtila, I.; Fanlo-Virgos, H.; Schaeffer, G.; Santiago, G. M.; Otto, S. *J. Am. Chem. Soc.* **2017**, *139*, 12459−12465.
(14) (a) Otsuki, J.; Suwa, K.; Sarker, K. K.; Sinha, C. *J. Phys. Chem. A* **2007**, *111*, 1403−1409. (b) Garcia-Amorós, J.; Reig, M.; Castro, M. C. R.; Cuadrado, A.; Raposob, M. M. M.; Velasco, D. *Chem. Commun.* **2014**, *50*, 6704−6706. (c) Calbo, J.; Weston, C. E.; White, A. J. P.; Rzepa, H. S.; Contreras-García, J.; Fuchter, M. J. *J. Am. Chem. Soc.* **2017**, *139*, 1261−1274. (d) Simeth, N. A.; Crespi, S.; Fagnoni, M.; König, B. *J. Am. Chem. Soc.* **2018**, *140*, 2940−2946.
(15) (a) Bromham, L.; Penny, D. *Nat. Rev. Genet.* **2003**, *4*, 216−224. (b) Kumar, S. *Nat. Rev. Genet.* **2005**, *6*, 654−662. (c) Lu, K. P.; Finn, G.; Lee, T. H.; Nicholson, L. K. *Nat. Chem. Biol.* **2007**, *3*, 619−629. (d) Lee, M. S. Y.; Ho, S. Y. W. *Curr. Biol.* **2016**, *26*, R399−R402.
(16) (a) Ray, D.; Foy, J. T.; Hughes, R. P.; Aprahamian, I. *Nat. Chem.* **2012**, *4*, 757−762. (b) Foy, J. T.; Ray, D.; Aprahamian, I. *Chem. Sci.* **2015**, *6*, 209−213. (c) Pramanik, S.; Aprahamian, I. *J. Am. Chem. Soc.* **2016**, *138*, 15142−15145. (d) Aprahamian, I. *Chem. Commun.* **2017**, *53*, 6674−6684.
(17) Qian, H.; Pramanik, S.; Aprahamian, I. *J. Am. Chem. Soc.* **2017**, *139*, 9140−9143.
(18) In **1** the H-bonds are with the ester carbonyl group ($d(N_2-O_1)$ = 2.631(3) Å, $\angle N_2-H\cdots O_1$ = 130.62°; $d(N_2-O_2)$ = 2.682(3) Å, $\angle N_2-H\cdots O_2$ = 129.91°) (Figure 1c), making a direct comparison difficult.
(19) While these values are relatively low, they are comparable to the ones obtained in other photochromic compounds, such as azobenzenes and diarylethenes.
(20) *p*-Xylene was used as the solvent in these studies because it has a high boiling point (138.4 °C), which allowed us to use a large range of temperatures during the rate measurements.
(21) (a) McCarthy, C. G. In *The Chemistry of the Carbon-Nitrogen Bond*; Patai, S., Ed.; John Wiley and Sons, New York, 1970; pp 392−399. (b) Parmerter, S. M. In *Organic Reactions*; Adam, R., Ed.; Wiley-VCH: New York, 1959; Vol. *10*, p 1. (c) Landge, S. M.; Tkatchouk, K.; Benitez, D.; Lanfranchi, D. A.; Elhabiri, M.; Goddard, W. A., III; Aprahamian, I. *J. Am. Chem. Soc.* **2011**, *133*, 9812−9823.
(22) Ponomarev, D. A. *J. Chem. Educ.* **1997**, *74*, 201−203.

DOI: 10.1021/jacs.8b07612
J. Am. Chem. Soc. 2018, 140, 11829−11835